

An alternative method of calculating cleavage energy: The effect of compositional domains in micas

MARIA FRANCA BRIGATTI^{1,*}, CHIARA ELMI², STEPHEN GUGGENHEIM³, DANIELE MALFERRARI¹, AND MARCO POPPI¹

¹Dipartimento di Scienze Chimiche e Geologiche, Università di Modena e Reggio Emilia, Via G.Campi 103, I-41125, Modena, Italy

²Department of Earth and Environmental Sciences, University of Pennsylvania, 240 South 33rd Street, Hayden Hall, Philadelphia, Pennsylvania 19104-6316, U.S.A.

³Department of Earth and Environmental Sciences, University of Illinois at Chicago, 845 West Taylor Street, Chicago 60607-7059, Illinois, U.S.A.

ABSTRACT

Cell parameters and atomic coordinates for the true micas are varied to simulate layer deformation along the [001]* direction by an external force. The resulting (deformed) structures are then used to determine bonding forces and to calculate a maximum force component along the [001]*. Bonding forces are compared to experimental observations of bond lengths of the interlayer, octahedral, and tetrahedral sites. Calculated bonding forces are consistent with experimental observations that locate the cleavage plane along the interlayer. Because many studies have shown that the chemical composition of the cleavage surface often differs from the structure of the bulk, compositional variations were considered in determining cleavage energy. The chemical composition of the cleavage surface may produce a reduction in cleavage energy. This reduction in energy depends on various elements occurring in greater number at the cleavage surface than in the bulk. A reduction in cleavage energy occurs if there is a reduction in the interlayer site size, as measured by the area defined by the first-coordination basal oxygen atoms. In addition, a reduction in lateral cell dimensions and an increase in the bonding force between the basal oxygen atoms and the interlayer cation also results in a reduction in cleavage energy in the direction normal to the layer.

Joins considered are phlogopite–annite, tetra-ferriphlogopite–tetra-ferri-annite, polyolithionite–siderophyllite, muscovite–celadonite, and muscovite–paragonite. A lack of homogeneity in composition may produce preferential cleavage locations within the family of (001) planes. The cleavage energy appears to be greater for homogeneous synthetic micas compared to natural micas.

Keywords: Micas, cleavage, electrostatic force, crystal chemistry, crystal structure

INTRODUCTION

Knowledge of the atomic arrangement of the topmost crystal surface of layer silicates is a requirement for the understanding of a large number of surface phenomena and the geochemical cycling of elements at the Earth's crust (Hochella 1990). Micas are of special interest because they are common phases in metamorphic, sedimentary, and igneous rocks and are used in many technological applications. The planar basal (001) surface, readily produced by cleavage, is ideally suited for numerous applications such as catalysts, sensors, automotive paints, cosmetics, ceramic pigments, and many others (Hochella 1995; Kogure et al. 2006; Maurice 2009; Andrić et al. 2014). The cleavage of mica is believed to occur at the interlayer, parallel to (001), and results in the exposure of K cations and/or vacant cation-exchange sites (Giese 1974, 1977, 1978). Giese (1974) suggested, from theoretical arguments, that muscovite cleaves along the interlayer and that K is regularly distributed on the two cleaved surfaces. This interpretation assumes that K is weakly bonded electrostatically to basal tetrahedral O atoms and is repulsed from other K atoms and the (OH) groups present in the ditrigonal cavity. Substitution of (OH) by F increases strength of the interlayer bonding (Giese 1977; Dahl and Dorais 1996). Some experimental studies (e.g., Poppa and Elliot 1971;

Kogure 1997; Biino and Gröning 1998; Elmi et al. 2013, 2014a, 2014b) relating bulk and surface crystal chemistry of the micas showed relaxation and reconstruction phenomena at the mica surface (e.g., variation of coordination number for the interlayer cation, preferential coordination for Mg to F compared with Mg to OH). In addition, these studies showed compositional variation from the bulk, such as K depletion and Si reduction from its highly oxidized state to the elemental state. Potassium depletion at the cleavage surface has been observed in all micas studied and this result is consistent with cleavage occurring by failure of interlayer cation to basal oxygen atom bonds (González-Elipe et al. 1988; Biino and Gröning 1998; Kogure 1997; Elmi et al. 2013, 2014a, 2014b). In addition, for Li-rich micas, an increase in Li content was observed near the (001) cleavage surface, thus suggesting a preference for cleavage near Li-enriched regions. Similarly, in muscovite, Na was observed to significantly increase at the cleavage surface (Elmi et al. 2013). At the surface of phengitic muscovite, Biino and Gröning (1998) observed an increase in Al content and in minor octahedral cations, such as Mg, with respect to the bulk. The authors suggested that cleavage may involve regions enriched with chlorite-like domains. In phlogopite, Evans et al. (1979) observed, at the cleavage surface, an increase in Al content at the expense of Mg, which is consistent also with the hypothesis of Biino and Gröning (1998).

* E-mail: mariafranca.brigatti@unimore.it

In the present work, we relate the properties of micas to atom distances, crystal structure, and crystal-chemical features. These properties are used to predict the effect of bulk-chemical composition, interlayer coordination, and compositional variations at the cleavage surface with respect to the cleavage process.

MODEL DERIVATION AND RELATED HYPOTHESES

The classical theory of ideal fracture in brittle materials, such as glass, is based on the stability of a crack in a homogeneous medium in a reversible thermodynamic system (Griffith 1921). The Griffith criterion states that a crack meets the critical growth condition when the net change in the total energy of the system ΔE vanishes upon crack extension by an infinitesimal distance Δa , thus $\Delta E = (G - 2\gamma_s) \Delta a = 0$, where G is the elastic energy release rate and γ_s is the surface energy density, which measures the fracture resistance of the material. The infinitesimal displacement Δa can be directed to induce an opening of the crack, in-plane shear, and out-of-plane shear, thus defining three elementary types of fracture, namely I, II, and III. For a model system with a crack of length $2a$ the Griffith fracture stress can be expressed as $\sigma'_G = \sqrt{2\gamma_s / \pi a}$ where Y denotes Young's modulus. The Griffith fracture stress has been widely used and improved (e.g., Pugno and Ruoff 2004; Zhang et al. 2007) to accurately predict cracks of ductile materials (Irwin 1957), and materials in different external environments (Parks 1984). Lazar et al. (2005) and Lazar and Podloucky (2008) presented a model for cleavage based on density functional theory calculations, which combines a purely elastic response with an abrupt breaking of the material. Within this model, two material parameters are introduced: the cleavage energy and the critical crack opening. The cleavage energy was derived from density functional theory calculations, in which the surfaces of the cleaved material are structurally relaxed. The critical crack opening was obtained by fitting the analytical model for the de-cohesive energy to density functional theory data (Elsner and Mueller 2015).

The cleavage energy of phyllosilicates has been addressed by some models. For example, Heinz et al. (2005) and Heinz (2006) derived a force-field model for mica-type silicates by considering atomic charges, van der Waals parameters, vibrational constants, and distributions of charge defects. The model predicts cleavage energy that deviates by <5% compared to experimental data. Heinz et al. (2013) introduced the "Interface force field" to enable simulation of inorganic-organic and inorganic-biomolecular interfaces. The method, that operates as an extension of common harmonic force fields, enables the quantitative assessment of a wide range of properties, for a wide range of minerals, including layer silicates.

The model discussed in this paper establishes relationships between atomic parameters, mostly related to the topology of the interlayer site, to cleavage processes. Model derivation addresses type I fracture mode (i.e., a normal force opening the layer) and starts by expressing relevant structural parameters, such as distances or angles, as a function of fractional coordinates and unit-cell parameters. The distance between two points is calculated as the root square of the scalar product of a vector \vec{V} pointing from the first point to the second. Calculation examples (Table 1), starting from this general definition and introducing symmetry constraints relative to the $1M$ polytype and $C2/m$ symmetry, are the distances between the interlayer cation A and individual basal

oxygen atoms (Fig. 1). A similar approach is used to express the force exchanged between the interlayer cation and basal oxygen atoms. The electrostatic interaction between electrically charged particles of charge q_1 and q_2 is calculated from the Coulomb law, as: $F = k_e \cdot (q_1 \cdot q_2) / |r_{12}|^3 \cdot r_{12}$ where k_e is Coulomb's constant, r_{12} is the vector pointing from the first charge to the second and $|r_{12}|$ is its magnitude.

Neglecting effects related to charge distribution, charge defects and the influence of external environment, we derive: $F_{A-O_i} \propto A-O_i / |A-O_i|^3$ where F_{A-O_i} is the force exchanged between the interlayer cation and one of its coordinated basal oxygen atoms O_i ; $A-O_i$ is the vector pointing from the interlayer cation to the basal oxygen atom O_i , and $|A-O_i|$ is the magnitude of the $A-O_i$ vector. The formulated hypotheses neglect parameters that significantly affect cleavage energy. However, linkages are made between crystal structural parameters (i.e., bond distances), that are also affected by some parameters not directly considered in the model, and the bond strength of the interlayer cation with neighboring basal oxygen atoms. The total force between the interlayer cation and basal oxygen atoms from a single layer is thus proportional to F_T , defined as: $F_T = \sum_{i=1}^6 A-O_i / |A-O_i|^3$. Therefore, F_T is related to the force by which the interlayer cation is bonded to the basal oxygen atoms as a function of the structural parameters only.

Similar to the discussion for $A-O_i$ distances (Table 1), the F_T and its component along $[001]^*$, F_N , are calculated using atomic coordinates and unit-cell parameters. This approach allows the

TABLE 1. Distance between the interlayer cation A and individual basal oxygen atoms calculated as the root square of the scalar product of a vector \vec{V} , pointing from interlayer cation to each basal oxygen atom. Symmetry constraints relative to the $1M$ polytype and $C2/m$ symmetry are introduced

$$A-O_{21} = \sqrt{\left(x_{O_2} \cdot a - \frac{1}{2}a - x_A \cdot a\right)^2 + \left(\frac{1}{2}b - y_{O_2} \cdot b - y_A \cdot b\right)^2 + (z_{O_2} \cdot c - z_A \cdot c)^2} + 2 \cdot \left(x_{O_2} \cdot a - \frac{1}{2}a - x_A \cdot a\right) \cdot (z_{O_2} \cdot c - z_A \cdot c) \cdot \cos(\beta) \quad (1)$$

$$A-O_{13} = \sqrt{\left(x_{O_1} \cdot a - \frac{1}{2}a - x_A \cdot a\right)^2 + \left(\frac{1}{2}b + y_{O_1} \cdot b - y_A \cdot b\right)^2 + (z_{O_1} \cdot c - z_A \cdot c)^2} + 2 \cdot \left(x_{O_1} \cdot a - \frac{1}{2}a - x_A \cdot a\right) \cdot (z_{O_1} \cdot c - z_A \cdot c) \cdot \cos(\beta) \quad (2)$$

$$A-O_{25} = \sqrt{\left(x_{O_2} \cdot a - \frac{1}{2}a - x_A \cdot a\right)^2 + \left(\frac{1}{2}b + y_{O_2} \cdot b - y_A \cdot b\right)^2 + (z_{O_2} \cdot c - z_A \cdot c)^2} + 2 \cdot \left(x_{O_2} \cdot a - \frac{1}{2}a - x_A \cdot a\right) \cdot (z_{O_2} \cdot c - z_A \cdot c) \cdot \cos(\beta) \quad (3)$$

$$A-O_{24} = \sqrt{\left(x_{O_2} \cdot a - x_A \cdot a\right)^2 + \left(b - y_{O_2} \cdot b - y_A \cdot b\right)^2 + (z_{O_2} \cdot c - z_A \cdot c)^2} + 2 \cdot \left(x_{O_2} \cdot a - x_A \cdot a\right) \cdot (z_{O_2} \cdot c - z_A \cdot c) \cdot \cos(\beta) \quad (4)$$

$$A-O_{12} = \sqrt{\left(x_{O_1} \cdot a + \frac{1}{2}a - x_A \cdot a\right)^2 + \left(\frac{1}{2}b + y_{O_1} \cdot b - y_A \cdot b\right)^2 + (z_{O_1} \cdot c - z_A \cdot c)^2} + 2 \cdot \left(x_{O_1} \cdot a + \frac{1}{2}a - x_A \cdot a\right) \cdot (z_{O_1} \cdot c - z_A \cdot c) \cdot \cos(\beta) \quad (5)$$

$$A-O_2 = \sqrt{\left(x_{O_2} \cdot a - x_A \cdot a\right)^2 + \left(y_{O_2} \cdot b - y_A \cdot b\right)^2 + (z_{O_2} \cdot c - z_A \cdot c)^2} + 2 \cdot \left(x_{O_2} \cdot a - x_A \cdot a\right) \cdot (z_{O_2} \cdot c - z_A \cdot c) \cdot \cos(\beta) \quad (6)$$

Note: x_{O_1} , y_{O_1} , z_{O_1} are atomic coordinates of the O1 oxygen atom; x_{O_2} , y_{O_2} , z_{O_2} are atomic coordinates of the O2 oxygen atom; x_A , y_A , z_A are atomic coordinates of the interlayer cation A and a , b , c , and β are unit-cell parameters.

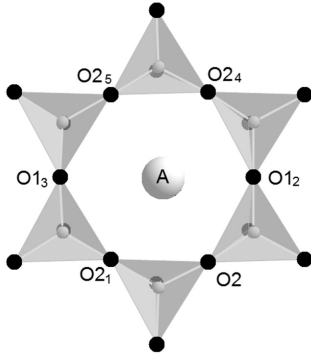


FIGURE 1. The tetrahedral hexagonal ring and identification of individual basal oxygen atoms.

determination of the changes of F_N as a function of the variation of atomic coordinates, of unit-cell parameters, or with any combination.

The derivation of the strain field associated with the application of an external force along $[001]^*$ is complex. For a force directed to mica $[001]^*$, a first-order approximation is obtained for the resulting deformation as an elongation of the structure along $[001]^*$, as simulated by an increase of the c cell parameter. Equivalently, because the bonding within the interlayer is weak compared to the 2:1 layer, the deformation may be described by an increase of the interlayer separation. Therefore, in this model, we express the F_N variation as a function of the unit-cell c parameter increase, and we assume that the other structural parameters (e.g., lateral cell parameters and fractional coordinates) are equal to values obtained from the crystal structure refinement under zero external force conditions.

The prediction of the F_N component and how it varies as a function of the c cell parameter increase is a good simulation of the strain field in micas subjected to an external force normal to the layer. Following this approach and using the phlogopite refinement from Russell and Guggenheim (1999) we derive:

$$F_N = \frac{0.46363 + 0.17130c}{(7.0586 + 0.29343c^2 + 0.15884c)^{3/2}} + \frac{0.17130c - 0.46178}{(7.002359 + 0.293437c^2 - 0.158206c)^{3/2}} + \frac{2(0.17140c + 0.1513976)}{(4.88399 + 0.2937796c^2 + 0.518991c)^{3/2}} + \frac{2(0.17140c - 0.311309)}{(9.7241677 + 0.2937796c^2 - 0.1067167c)^{3/2}}$$

The variation of F_N identifies a maximum force value ($F_{N,Max}$), with an increase in the c cell parameter (or interlayer separation) and this value is greater than the initial F_N (Fig. 2). The initial F_N implies that the structure has not deformed by an external force normal to the layer. The $F_{N,Max}$ allows a direct comparison of the attractive forces of the interlayer cation and basal oxygen atoms even for mica crystals of different layer symmetry or different chemical composition, as determined by atomic distances.

Examples discussed in this section refer to 1M polytype ($C2/m$ symmetry), but the same approach applies to other polytypes (e.g., 1M in $C2$ symmetry) and to dioctahedral micas- $2M_1$ belonging to $C2/c$ symmetry, which are discussed below.

INTERLAYER SITE

Experimental data confirm that cleavage occurs at the (001) plane (Kuwahara 2001; Guidotti et al. 2005) thus showing the

significant role of interlayer topology and composition. The detachment of two adjacent layers along the direction normal to the layer (i.e., $[001]^*$) is described by the Coulomb force exerted by interlayer cations on the basal oxygen atoms of the mating layers. The force is proportional to $\overline{F}_i = \sum_{i=1}^6 \frac{A-O_i}{|A-O_i|^3}$, assuming a coordination of six and an interlayer charge equal to 1 for true micas, where A is the interlayer cation and O_i is a basal oxygen atom coordinated to A and belonging to one of the two mating tetrahedral sheets.

When an external force along $[001]^*$ is applied, the structure will deform with an increase in interlayer separation. This force component is neither monotonic nor decreasing, unlike the electrostatic potential associated with the interlayer cation that monotonically decreases as interlayer separation increases.

Plots shown in Figure 2 represent end-member compositions of true mica-1M polytypes, together with some mica plots where surface composition and topology are available. All trends show an initial value at zero deformation (i.e., $F_{N,i}$), a maximum value (i.e., $F_{N,Max}$) and the deformation value, where $F_{N,Max}$ is observed (i.e., D_{Max}). Note that phlogopite, Li-rich siderophyllite, and tetra-ferriphlogopite have similar values of $F_{N,i}$, whereas tetra-ferriphlogopite shows a different behavior for the evolution of F_N as a function of deformation, with a lower $F_{N,Max}$ value. These trends also identify an evident variation of F_N as a function of chemical composition. In particular, for phlogopite and annite, an increase in octahedral Fe content marks a decrease in F_N . For Fe-rich polythionite vs. Li-rich siderophyllite, an increase in octahedral Fe content at the expense of Li produces lower values in F_N .

For mica-1M in the phlogopite-annite and tetra-ferriphlogopite-tetra-ferril-annite joins, Figure 3 shows the variation of $F_{N,Max}$ as a function of $[^{VI}Fe^{2+}]$ content. This plot shows a decrease in $F_{N,Max}$ with a $[^{VI}Fe^{2+}]$ increase. The $F_{N,Max}$ increases in the polythionite-siderophyllite join ($C2$ symmetry, 1M polytype) with increasing $[^{VI}Li]$ and $[^{VI}Al^{3+}]$ and decreasing $[^{VI}Fe^{2+}]$ (Fig. 4). These data suggest that, at a fixed interlayer site charge, interlayer cations are more

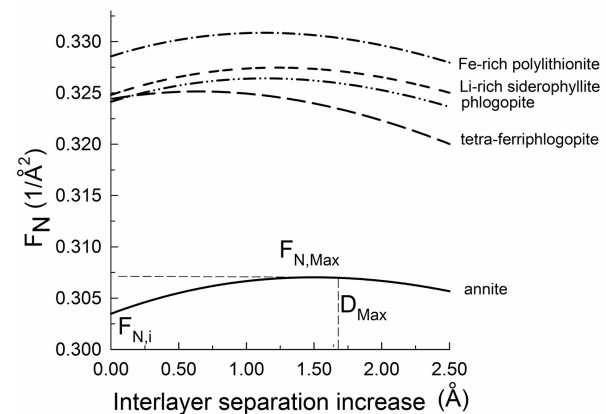


FIGURE 2. Variation of F_N (i.e., \overline{F}_i component along $[001]^*$) as a function of c cell parameter (or interlayer separation) increase. Plots for the designated end-members include a much larger data set involving intermediate compositions. Samples: annite (Brigatti et al. 2000a), tetra-ferriphlogopite (Elmi et al. 2014a), phlogopite (Russell and Guggenheim 1999), Li-rich siderophyllite (Elmi et al. 2014b), and Fe-rich polythionite (Elmi et al. 2014b).

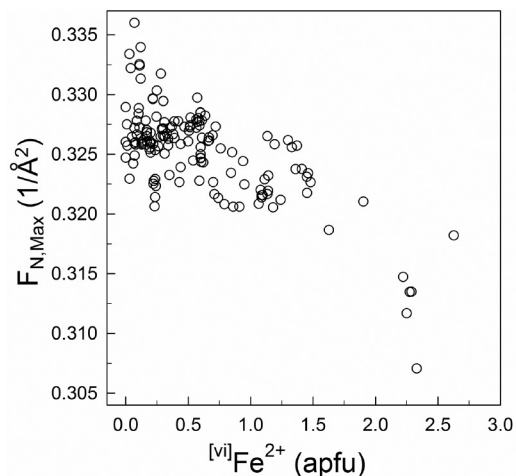


FIGURE 3. Variation of $F_{N,Max}$ (i.e., F_N at the maximum point, Fig. 2) as a function of octahedral $[^{iv}]Fe^{2+}$ content for trioctahedral micas-1M in phlogopite-annite and tetra-ferriphlogopite-tetra-ferriferri-annite joins. Samples are from: Alietti et al. (1995); Bigi and Brigatti (1994); Brigatti and Davoli (1990); Brigatti and Poppi (1993); Brigatti et al. (1991, 1996, 2000a, 2000b, 2001a, 2005b, 2007a); Elmi et al. (2014a); Gianfagna et al. (2007); Hazen et al. (1981); Hazen and Burnham (1973); Laurora et al. (2007, 2009); Ohta et al. (1982); Matarrese et al. (2008); McCauley et al. (1973); Redhammer and Roth. (2002); Russell and Guggenheim (1999); Schingaro et al. (2005); Scordari et al. (2006, 2008).

strongly bonded to basal oxygen atoms in polyolithionite as compared to siderophyllite, and in phlogopite as compared to annite.

Elmi et al. (2014b) observed a Li increase at the cleaved surface of Li-rich micas with respect to the bulk, thus demonstrating surface enrichment in an element that shows an increase in $F_{N,Max}$. In the polyolithionite-siderophyllite 1M join, $F_{N,Max}$ increases with tetrahedral $[^{iv}]Si$ content and decreases with tetrahedral $[^{iv}]Al$ content (Fig. 5). Similar trends do not occur in the phlogopite-annite and tetra-ferriphlogopite-tetra-ferriferri-annite joins. This result relates to a strong dependence between $F_{N,Max}$ and the area of the hexagon defined by the basal oxygen atoms. A smaller area and, more generally, smaller lateral a and b dimensions, result in a greater $F_{N,Max}$ (Figs. 6 and 7).

Figure 6 illustrates an expected trend because the greater the attraction of the interlayer cation for the oxygen atoms defining its coordination results in a smaller interlayer site. Thus, $\langle A-O \rangle_{inner}$ distances define a similar trend as the one observed in Figure 6. Less obvious is the trend in Figure 7 where the lateral cell parameter a shows a dependence on the interlayer cation coordination that affects the entire layer. In micas of the polyolithionite-siderophyllite join, this relationship suggests the reduction in size of the tetrahedral and octahedral sites, thus giving a $F_{N,Max}$ increase with $[^{iv}]Si$ content and decreases with $[^{iv}]Al$ content. Furthermore the average angle defined by the bond of interlayer cation to basal oxygen atoms with respect to c^* is observed to decrease with $F_{N,Max}$ increase, thus suggesting that the effect of lateral cell dimension reduction, which accounts for a reduction of the angle at same interlayer separation, is proportionally stronger than reduction in interlayer separation, which would account for an increase of angle at same lateral cell dimensions (Fig. 8a).

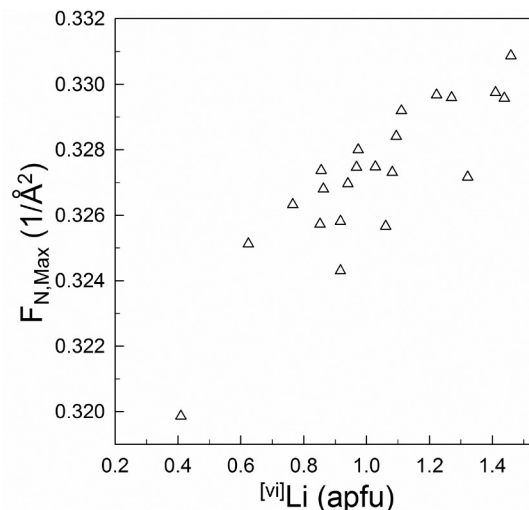


FIGURE 4. Variation of $F_{N,Max}$ as a function of octahedral $[^{iv}]Li^+$ content for micas-1M in the polyolithionite-siderophyllite join. Samples are from Brigatti et al. (2000a, 2007b) and Elmi et al. (2014b).

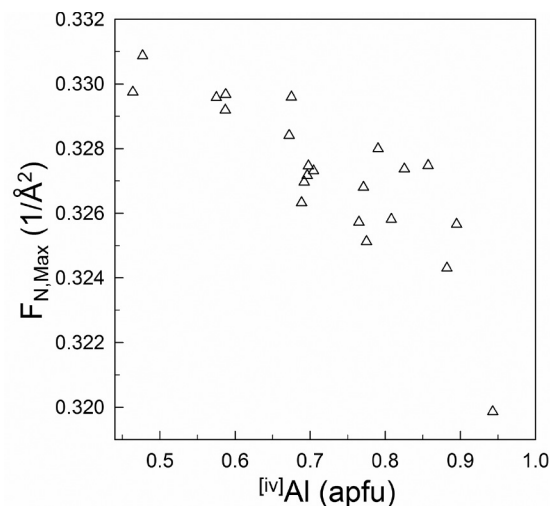


FIGURE 5. Variation of $F_{N,Max}$ as a function of tetrahedral $[^{iv}]Al$ content. Samples as in Figure 4.

In micas of the phlogopite-annite and tetra-ferriphlogopite-tetra-ferriferri-annite joins, the decrease in both octahedral size and interlayer site size are caused by a topology change of the basal oxygen plane, as measured by the tetrahedral rotation angle α and not by a reduction in the area defined by tetrahedral basal oxygen atoms. The α angle value, unlike what is observed for micas of the polyolithionite-siderophyllite join, is directly correlated to $F_{N,Max}$ (Fig. 8b).

In micas of the polyolithionite-siderophyllite join, a direct although imperfect correlation is observed between F content and $F_{N,Max}$ (Fig. 9a). The trend is related to the reduction of the interlayer site size. This result occurs because of the inverse relationship observed between F and $[^{iv}]Fe^{2+}$ content (Fig. 9b).

Figure 10 shows the variation of F_N as a function of the c cell parameter (or interlayer separation) for two dioctahedral micas

belonging to the $2M_1$ polytype (space group $C2/c$). Muscovite and paragonite are shown. Note that $F_{N,Max}$ values are higher for dioctahedral micas- $2M_1$ (Fig. 10) compared to trioctahedral micas- $1M$ (Fig. 2). This result is related to the smaller lateral cell dimension and to the size of the interlayer cation site in dioctahedral micas

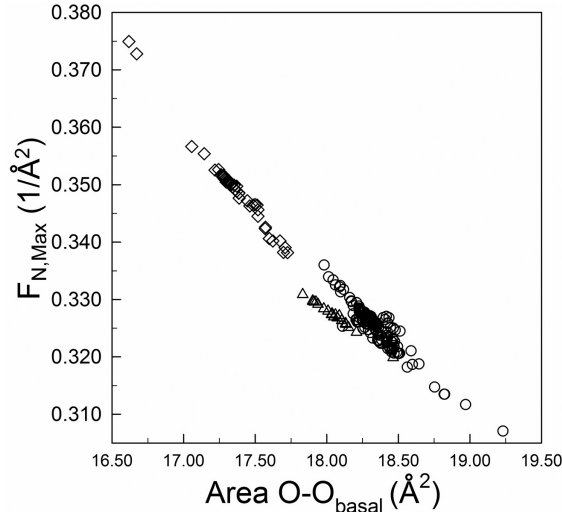


FIGURE 6. Influence of $F_{N,Max}$ over the area of the hexagon defined by basal oxygen atoms. Symbols: circles = trioctahedral micas of the phlogopite-annite and tetra-ferriphlogopite-tetra-ferri-annite joins; triangles = trioctahedral micas of the polyolithionite-siderophyllite join; diamonds = dioctahedral micas of the muscovite-paragonite join. Samples: Alietti et al. (1995); Benincasa et al. (2003); Bigi and Brigatti (1994); Brigatti and Davoli (1990); Brigatti and Poppi (1993); Brigatti et al. (1991, 1996, 1998, 2000a, 2000b, 2001a, 2001b, 2001c, 2005a, 2005b, 2007a, 2007b, 2008); Comodi and Zanazzi (1997); Elmi et al. (2013, 2014a, 2014b); Gianfagna et al. (2007); Guggenheim et al. (1987); Guven (1971); Hazen and Burnham (1973); Hazen et al. (1981); Laurora et al. (2007, 2009); Lin and Bailey (1984); Matarrese et al. (2008); McCauley et al. (1973); Ohta et al. (1982); Redhammer and Roth (2002); Russell and Guggenheim (1999); Schingaro et al. (2005); Scordari et al. (2006, 2008).

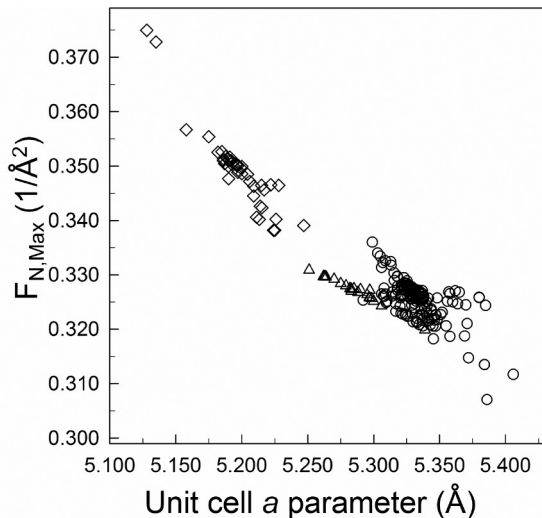


FIGURE 7. Influence of $F_{N,Max}$ from lateral cell parameter a . Symbols and samples as in Figure 6.

as compared to trioctahedral micas (Figs. 6 and 7).

The substitution of Na for K in the interlayer that defines the muscovite-paragonite join produces a reduction in interlayer site size (Fig. 11a) and an increase in $F_{N,Max}$ (Fig. 11b). Surface studies for an analyzed muscovite sample with limited Na for K substitution show that Na content increases at the cleavage surface (Elmi et al. 2013). In this mica, similar to what is observed in Li-rich trioctahedral micas, the cleavage surface is enriched with elements that produce a reduced lateral cell dimension, reduced size of the interlayer site, and an increased attractive force of the basal oxygen atoms to the interlayer cation. Similarly, greater $F_{N,Max}$ values observed in muscovite are related to greater Al content and a reduced Mg content at the cleavage surface, as compared to the bulk of phlogopite (Evans et al. 1979), clinocllore, or penninite (Evans and Hiorns 1996).

Gutshall et al. (1970) measured the cleavage energy of phlogopite at 3630 erg/cm² for a natural sample in a vacuum of 10⁻⁷ Tor.

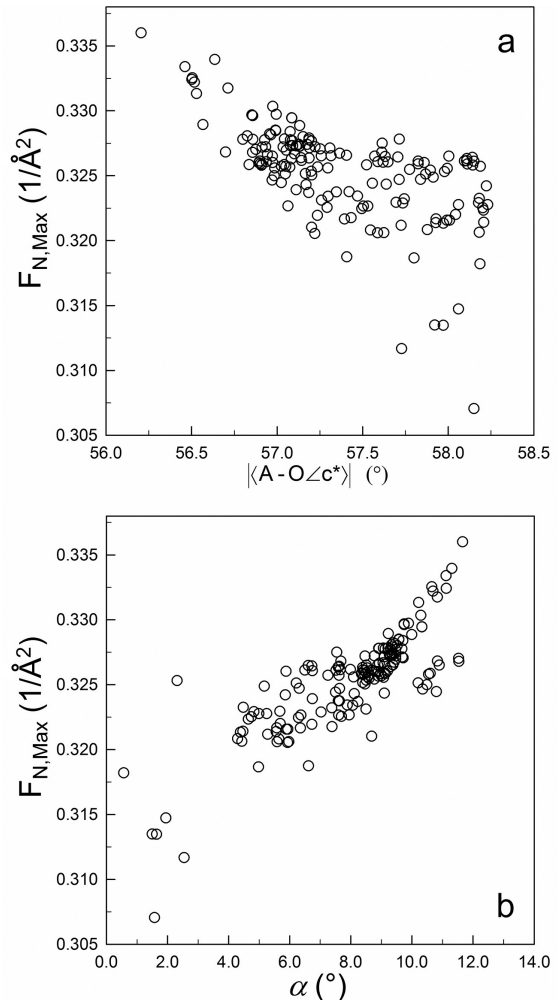


FIGURE 8. Plot of $F_{N,Max}$ vs.: (a) angle $\langle A-O\angle c^* \rangle$, where $\langle A-O\angle c^* \rangle = \sum_{i=1}^6 (A-O\angle c^*)/6$ is the average of individual angles defined by A-O, bonds with respect to c^* and O, defines an individual basal oxygen atom coordinated to the interlayer cation A and (b) α angle for trioctahedral micas- $1M$ in the phlogopite-annite and tetra-ferriphlogopite-tetra-ferri-annite joins. Samples as in Figure 3.

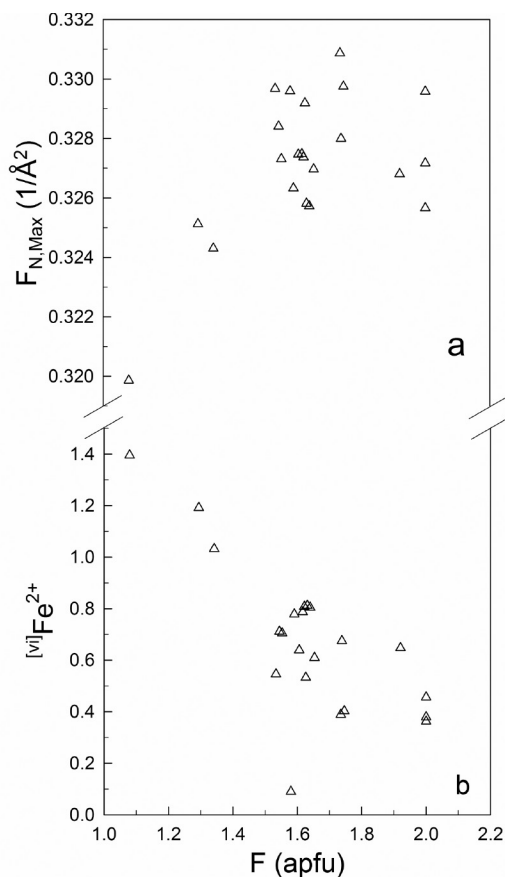


FIGURE 9. Trioctahedral micas-1M in polyolithionite-siderophyllite join: influence of F in the anion site over: (a) $F_{N,Max}$ and (b) octahedral Fe^{2+} . Samples as in Figure 4.

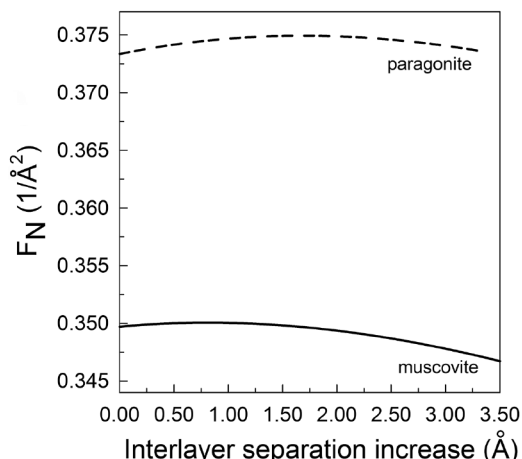


FIGURE 10. Variation of F_N (i.e., \overline{F}_T component along $[001]^*$) as a function of c cell parameter (or interlayer separation). Plots for the designated end-members include a much larger data set involving intermediate compositions. Solid line = muscovite (Elmi et al. 2013); dashed line = paragonite (Lin and Bailey 1984).

The cleavage energy increased to 6060 erg/cm² in vacuum for a synthetic sample, with the difference interpreted by the authors to be related to “impurities” in the natural sample. Parks (1984)

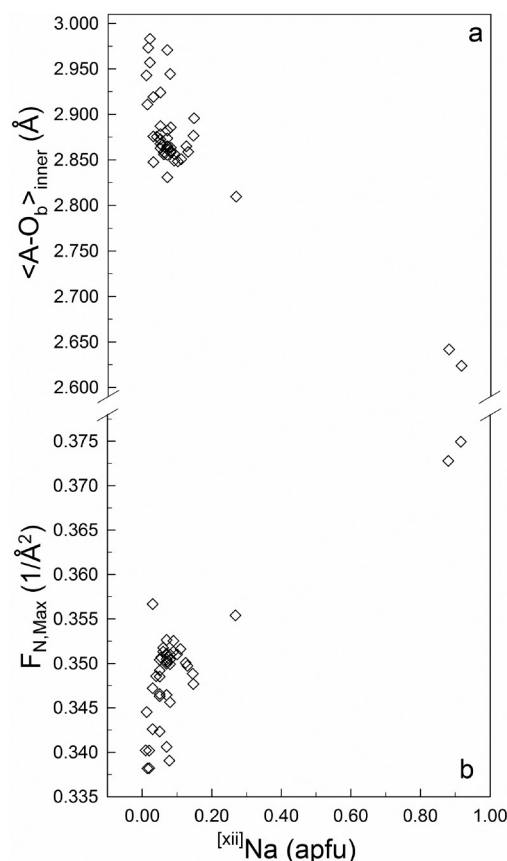


FIGURE 11. Dioctahedral $2M_1$ micas in the muscovite-paragonite join. (a) Variation of inner distances ($A-O_b$) vs. Na; (b) increase of $F_{N,Max}$ vs. Na content (apfu, atoms per formula unit). Samples: Benincasa et al. (2003); Brigatti et al. (1998, 2001b, 2001c, 2008); Comodi and Zanazzi (1997); Elmi et al. (2013); Guggenheim et al. (1987); Guven (1971); Lin and Bailey (1984).

demonstrated that water and electrolytes cause significant changes in the fracture strength of silicates. Experimental surface fracture energies of micas range from about 183 erg/cm² in the presence of water vapor and 5125 erg/cm² in a vacuum. Thus, the reaction of water vapor with elements at the pristine surface fracture reduce the surface energy by hydroxylation. Heinz et al. (2005) demonstrated that the highest cleavage energy is related to rapidly induced cleavage on (001) and it involves an unequal partition of K ions between adjacent surfaces; if mica is cleaved slowly so that K cations are equally partitioned between the newly formed surfaces, the cleavage energy decreases from 4500 to 375 erg/cm². These differences occur because net charges are generated on the opposite surfaces, which produce a distance dependence of the interaction energy (Giese 1974). Furthermore Giese (1977), using the distance least-square method, calculated the surface energy as a function of interlayer separation. He observed an increasing surface energy for dioctahedral micas when compared to trioctahedral micas, which is consistent with data previously reported.

The enrichment at the mica surface of elements that reduce the interlayer-site size and thus reduce the lateral cell dimensions is caused by relaxation that affects cleavage surfaces. These processes produce the a and b cell dimension changes that show

gradual and regular shortening and elongation at the surface (e.g., Kuwahara 2001). The effect of layer structure on chemical substitutions, which induces an increase in F_N , is schematically represented in Figure 12. To illustrate, the Na for K interlayer substitution is shown. The Na for K substitution reduces interlayer separation [from 3.888 Å in muscovite (Guggenheim et al. 1987) to 3.074 Å in paragonite (Comodi and Zanazzi 1997)], $\langle A-O \rangle_{\text{inner}}$ distances [from 2.858 Å in muscovite (Guggenheim et al. 1987) to 2.634 Å in paragonite (Comodi and Zanazzi 1997)] and increases tetrahedral ring distortion (α angle) [from 11.3° in muscovite (Guggenheim et al. 1987) to 16.2° in paragonite (Comodi and Zanazzi 1997)]. Because each basal oxygen atom belongs to two adjacent interlayer rings, the effect of Na for K substitution will give intermediate values than observed in paragonite and muscovite. In this way, the ring occupied by K interlayer cation will show an increase in $\langle A-O \rangle_{\text{outer}}$ distances if its adjacent rings are occupied by Na (Fig. 12a). This mechanism also involves an increase in the α angle for the ring occupied by K, thus stressing dimensional matching between tetrahedral and octahedral site, since $\alpha = \cos^{-1} \sqrt{3} / 2 \cdot \langle O3-O3 \rangle / \langle O-O \rangle_{\text{basal}}$ where $\langle O3-O3 \rangle$ is the mean octahedral edge and $\langle O-O \rangle_{\text{basal}}$ is the mean basal tetrahedral O-O distance (Brigatti et al. 2003). Furthermore, the reduction in interlayer separation following Na for K substitution may induce a displacement or deformation of the layer marking an increase in interlayer separation for adjacent K interlayers (Fig. 12b). All the mechanisms described above can cooperate together to give a traction strain that promotes cleavage.

The trends in Figure 11 show an apparent compositional gap because the Na content ranging from 0.4 to 0.8 atom per formula unit is not represented. True compositional gaps are observed, however, for octahedral Al content in trioctahedral micas and for Mg, Fe content in dioctahedral micas (Brigatti et al. 2005a). These samples are characterized by different $F_{N,\text{Max}}$ values. A possible explanation for these compositional gaps may be the requirement of matching different lateral cell dimension along the stacking direction.

As noted above, the cleavage energy of phlogopite is reported to range from approximately 200 erg/cm² in water vapor to 4500 erg/cm² in vacuum. Using Coulombic calculations, the $F_{N,\text{Max}}$ for the interlayer cation to basal oxygen for phlogopite (Russell and Guggenheim 1999), [i.e., $0.3395 \times 10^{20} \text{ m}^{-2}$, is multiplied by the Coulomb constant $k_c = 8.987 \times 10^9 \text{ N} \times \text{m}^2 / \text{C}^2$, and by the second power of the elementary charge, $1.6 \times 10^{-19} \text{ C}$], can be used to estimate the maximum attractive force component along $[001]^*$. Force magnitude is divided by $a \times b$ (i.e., $48.7 \times 10^{-20} \text{ m}^2$) to obtain force per unit area and multiplied by a displacement set equal to the covalent oxygen radius (i.e., $0.73 \times 10^{-10} \text{ m}$). The result is the energy required to produce the displacement equal to the covalent oxygen radius. Based on the trends in Figure 2, F_N is nearly constant and equal to $F_{N,\text{Max}}$ for displacement values equal to the covalent oxygen radius. The determined energy value required for imparting a displacement to the layer equal to the covalent oxygen radius is 1.152 J/m² or equivalently 1152 erg/cm². This value is the same order of magnitude as that of the energy determined experimentally (Gutshall et al. 1970; Giese 1977; Heinz et al. 2005). The observed reduction of cleavage energy at ambient pressure may be related to the interaction of air with the mica structure because the experimentally derived cleavage energy is comparable to the

energy required to increase interlayer separation by a distance equal to the covalent oxygen radius.

TETRAHEDRAL AND OCTAHEDRAL SITES

An approach similar to the derivation of $F_{N,\text{Max}}$ at the interlayer site is applied here to the tetrahedral and octahedral sites. The tetrahedral cation is attracted to basal oxygen atoms with a force proportional to $F_{T,\text{basal}} = \sum_{i=1}^3 Q_T \left(\frac{T-O_i}{|T-O_i|} \right)^3$, where T is the tetrahedral cation, O_i are tetrahedral basal oxygen atoms bonded to T, and Q_T is the charge of the tetrahedral cation, which is introduced to allow a qualitative comparison to values obtained for the interlayer site. Obtained vectors are projected along $[001]^*$ to assess the response of the site for an external force applied along $[001]^*$, thus leading to the definition of $F_{T,\text{basal},N}$ and of $F_{T,\text{apical},N}$. Similarly, $F_M = \sum_{j=1}^3 Q_M \left(\frac{M-O_j}{|M-O_j|} \right)^3$, where Q_M is the charge of the octahedral cation M (M1 or M2), and O_j are its three coordinated oxygen atoms that define a face of the octahedron normal to $[001]^*$ (i.e., $F_{M1,N}$, $F_{M2,N}$).

Using the structure refinement of phlogopite (Russell and Guggenheim 1999) as an example, Figure 13 shows trends for

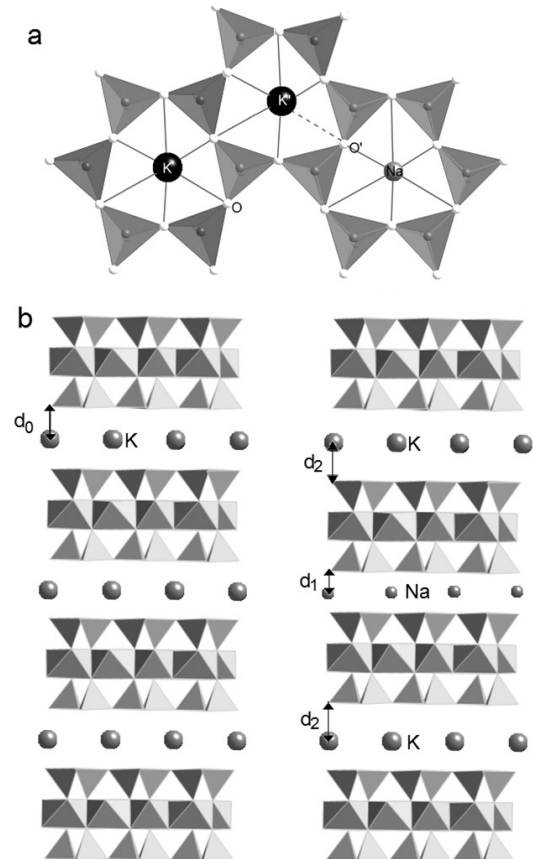


FIGURE 12. Mechanism describing the variation in interlayer distances produced by a Na-rich domain in muscovite. (a) Variation of K-O bond lengths ($K-O < K'-O'$) on (001). (b) Variation of K-O bond length along $[001]^*$. d_0 represents the distance between K and basal tetrahedral plane in muscovite (approximately 1.70 Å); d_1 represents the distance between Na and basal tetrahedral plane in paragonite (~1.54 Å); d_2 represents the increased distance between K and basal tetrahedral plane in K interlayers near the Na-rich domain. Note that: $d_1 < d_0 < d_2$.

$F_{T, \text{basal}, N}$ and for $F_{T, \text{apical}, N}$ as a function of tetrahedral deformation along $[001]^*$. The trend of $F_{T, \text{basal}, N}$ shows values three to four times greater than $F_{N, \text{Max}}$, which is the attractive force of the interlayer cation to basal oxygen atoms along $[001]^*$. Because the tetrahedral sites are present in a ratio of 4 to 1 with respect to interlayer sites, the force required to break the bonds between the tetrahedral cations and the basal oxygen atoms is more than one order of magnitude greater than the force required to break the bonds between the basal oxygen atoms and their coordinating interlayer cations. This result is consistent with the experimentally observed cleavage mechanism involving the interlayer site. Also $F_{T, \text{apical}, N}$ is more than one order of magnitude greater than $F_{N, \text{Max}}$, however decreasing with increasing deformation along $[001]^*$. The $F_{M1, N}$ and $F_{M2, N}$ values, calculated using Mg octahedral occupancy (phlogopite), are approximately twice that of $F_{N, \text{Max}}$. The ratio increases to approximately six for the phlogopite structure because the octahedral and interlayer sites are present in a ratio of 3:1. When octahedral deformation occurs following the application of an external force along $[001]^*$, both $F_{M1, N}$ and $F_{M2, N}$ slightly increase, see Figure 13.

All reported data are consistent with experimental observations that locate the (001) cleavage plane on the interlayer site. Thus, the observed variation in Si coordination at the mineral surface (Elmi et al. 2013) is related to surface relaxation and reconstruction effects following cleavage.

IMPLICATIONS

The bonding force between cations and coordinating oxygen anions in the mica structure can be expressed, in a first approximation, as a function of cell parameters and atomic coordinates. By varying these structural parameters, the variation in bonding force may be simulated as a consequence of layer deformations associated to an external action. This approach involves defining a maximum force component, $F_{N, \text{Max}}$ of the interlayer

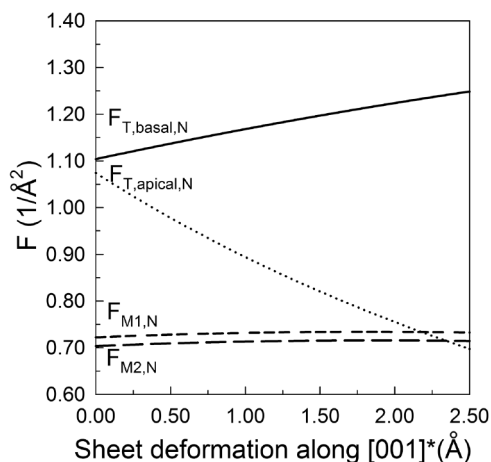


FIGURE 13. Variation of $F_{T, \text{basal}, N}$ (solid line) and $F_{T, \text{apical}, N}$ (dotted line) as a function of tetrahedral site deformation along the $[001]^*$ direction, and of $F_{M1, N}$ (short dashed line) and of $F_{M2, N}$ (long dashed line) as a function of octahedral site deformation along the $[001]^*$ direction. Tetrahedral ^{IV}Al occupancy and octahedral ^{VI}Mg occupancy are considered. Values are obtained by using phlogopite from Russell and Guggenheim (1999) as the example.

cation, interacting with basal oxygen atoms when applying a deformation along $[001]^*$. $F_{N, \text{Max}}$ is inversely related to the lateral cell dimensions and to interlayer site size.

Based on previous data, the cleavage surface in micas is enriched in elements that increase $F_{N, \text{Max}}$, if compared to the composition of the bulk. This result is consistent with a lack of homogeneity of the layers constituting the mica structure, with chemical substitutions concentrating in domains not regularly distributed in the layer that may contribute in starting the cleavage process. The enrichment of certain chemical elements at the cleavage surface produces an increased $F_{N, \text{Max}}$ and smaller interlayer site sizes. The latter is measured by the area defined by tetrahedral basal oxygen atoms. These chemical elements are probably associated with relaxation processes observed on the cleavage plane of micas, where lateral cell dimensions vary gradually by either small increases or decreases in length.

Technical applications that exploit the cleavage properties of micas that may potentially benefit from these results because cleavage location, and probably the force required to induce cleavage, may be controlled by chemical substitutions of elements in the mica. The appropriate chemical substitutions will give greater $F_{N, \text{Max}}$ values, which can thus act to start/initiate the cleavage process. The result of cleavage in micas is crystals with different features and properties at the surface with respect to the bulk. The ability to control chemical composition at the surface and in the bulk may provide opportunities to develop innovative materials with optimized physical and chemical properties (e.g., electrically conductive materials at the surface and insulator in the bulk). Furthermore, control of cleavage energy could lead to numerous technological applications such as the production of components that fail when subjected to a particular strain value, controlled by chemical composition. Such materials could be used to limit mechanical energy adsorbed in a system.

Finally when studying alteration processes affecting mica-bearing rocks, it should be considered that average chemical composition of mica samples may not be fully representative of the composition observed at the surface. The results introduced in this paper provide a qualitative indication of how the chemical composition observed on a freshly cleaved mica surface interacts with the surrounding environment.

ACKNOWLEDGMENTS

We are grateful and appreciate associate editor Callum Hetherington for assistance received during the revision process, and Hendrik Heinz and Alessandro Pavese who provided thoughtful and supportive reviews of the manuscript.

REFERENCES CITED

- Alietti, E., Brigatti, M.F., and Poppi, L. (1995) The crystal structure and chemistry of high-aluminium phlogopite. *Mineralogical Magazine*, 59, 149–157.
- Andrić, L., Terzić, A., Aćimović-Pavlović, Z., Pavlović, L., and Petrov, M. (2014) Comparative kinetic study of mechanical activation process of mica and talc for industrial application. *Composites: Part B*, 59, 181–190.
- Benincasa, E., Brigatti, M.F., Poppi, L., and Bea, F. (2003) Crystal chemistry of dioctahedral micas from peraluminous granites: the Pedrobernardo pluton (Central Spain). *European Journal of Mineralogy*, 15, 543–550.
- Bigi, S., and Brigatti, M.F. (1994) Crystal chemistry and microstructures of plutonic biotite. *American Mineralogist*, 79, 63–72.
- Biino, G.G., and Gröning, P. (1998) Cleavage mechanism and surface chemical characterization of phengitic muscovite and muscovite as constrained by X-ray Photoelectron Spectroscopy. *Physics and Chemistry of Minerals*, 25, 168–181.
- Brigatti, M.F., and Davoli, P. (1990) Crystal structure refinement of 1M plutonic biotites. *American Mineralogist*, 75, 305–313.
- Brigatti, M.F., and Poppi, L. (1993) Crystal chemistry of Ba-rich trioctahedral micas-1M. *European Journal of Mineralogy*, 5, 857–871.

- Brigatti, M.F., Galli, E., and Poppi, L. (1991) Effect of Ti substitution in biotite-1M crystal chemistry. *American Mineralogist*, 76, 1174–1183.
- Brigatti, M.F., Medici, L., Sacconi, E., and Vaccaro, C. (1996) Crystal chemistry and petrologic significance of Fe³⁺-rich phlogopite from the Tapira carbonatite complex, Brazil. *American Mineralogist*, 81, 913–927.
- Brigatti, M.F., Frigieri, P., and Poppi, L. (1998) Crystal chemistry of Mg-, Fe²⁺-bearing muscovites-2M₁. *American Mineralogist*, 83, 775–785.
- Brigatti, M.F., Lugli, C., Poppi, L., Foord, E.E., and Kile, D.E. (2000a) Crystal chemical variations in Li- and Fe-rich micas from Pikes Peak Batholith (central Colorado). *American Mineralogist*, 85, 1275–1286.
- Brigatti, M.F., Frigieri, P., Ghezzi, C., and Poppi, L. (2000b) Crystal chemistry of Al-rich biotites coexisting with muscovites in peraluminous granites. *American Mineralogist*, 85, 436–448.
- Brigatti, M.F., Medici, L., Poppi, L., and Vaccaro, C. (2001a) Crystal chemistry of trioctahedral micas-1M from Alto-Paranaíba igneous province, South-Eastern Brazil. *Canadian Mineralogist*, 39, 1333–1345.
- Brigatti, M.F., Kile, D.E., and Poppi, M. (2001b) Crystal structure and chemistry of lithium-bearing muscovite-2M₁. *Canadian Mineralogist*, 39, 1171–1180.
- Brigatti, M.F., Galli, E., Medici, L., Poppi, L., Cibin, G., Marcelli, A., and Mottana, A. (2001c) Chromium-containing muscovite: crystal chemistry and XANES spectroscopy. *European Journal of Mineralogy*, 13, 377–389.
- Brigatti, M.F., Guggenheim, S., and Poppi, M. (2003) Crystal chemistry of the 1M mica polytype: The octahedral sheet. *American Mineralogist*, 88, 667–675.
- Brigatti, M.F., Malferrari, D., Poppi, M., and Poppi, L. (2005a) The 2M₁ dioctahedral mica polytype: A crystal chemical study. *Clays and Clay Minerals*, 53, 190–197.
- Brigatti, M.F., Caprilli, E., Funicello, R., Giordano, G., Mottana, A., and Poppi, L. (2005b) Crystal chemistry of ferroan phlogopites from the Albano maar lake (Colli Albani volcano, central Italy). *European Journal of Mineralogy*, 17, 611–621.
- Brigatti, M.F., Caprilli, E., Malferrari, D., and Mottana, A. (2007a) Crystal structure and crystal chemistry of fluorannite and its relationships to annite. *Mineralogical Magazine*, 71, 683–690.
- Brigatti, M.F., Mottana, A., Malferrari, D., and Cibin, G. (2007b) Crystal structure and chemical composition of Li-, Fe-, and Mn-rich micas. *American Mineralogist*, 92, 1395–1400.
- Brigatti, M.F., Guidotti, C.V., Malferrari, D., and Sassi, F.P. (2008) Single-crystal X-ray studies of trioctahedral micas coexisting with dioctahedral micas in metamorphic sequences from western Maine. *American Mineralogist*, 93, 396–408.
- Comodi, P., and Zanazzi, P.F. (1997) Pressure dependence of structural parameters of paragonite. *Physics and Chemistry of Minerals*, 24, 274–280.
- Dahl, P.S., and Dorais, M.J. (1996) Influence of F(OH)₁ substitution on the relative mechanical strength of rock forming micas. *Journal of Geophysical Research* 101, 11,519–11,524.
- Elmi, C., Brigatti, M.F., Guggenheim, S., Pasquali, L., Montecchi, M., Malferrari, D., and Nannarone, S. (2013) Sodian muscovite-2M₁: crystal chemistry and surface features. *Canadian Mineralogist*, 51, 5–14.
- Elmi, C., Brigatti, M.F., Guggenheim, S., Pasquali, L., Montecchi, M., and Nannarone, S. (2014a) Crystal chemistry and surface configurations of two iron-bearing trioctahedral mica-1M polytypes. *Clays and Clay Minerals*, 62, 243–252.
- (2014b) Crystal chemistry and surface configurations of two polyolithionite-1M crystals. *American Mineralogist*, 99, 2049–2059.
- Elsner, B.A.M., and Mueller, S. (2015) Size effects and strain localization in atomic-scale cleavage modeling. *Journal of Physics: Condensed Matter*, 27, 1–8.
- Evans, S.F., and Hiorns, A. (1996) Angle-resolved X-ray Photoelectron studies of cleavage in chlorites. *Clays and Clay Minerals*, 44, 398–407.
- Evans, S.F., Raftery, E., and Thomas, J.M. (1979) Angular variation in core-level XPS-peak intensity ratios from single crystal solids. *Surface Science*, 89, 64–75.
- Gianfagna, A., Scordari, F., Mazzioni-Tagliani, S., Ventruti, G., and Ottolini, L. (2007) Fluorophlogopite from Biancavilla (Mt. Etna, Sicily, Italy): Crystal structure and crystal chemistry of a new F-dominant analog of phlogopite. *American Mineralogist*, 92, 1601–1609.
- Giese, R.F. Jr. (1974) Surface energy calculations for muscovite. *Nature*, 248, 580–581.
- (1977) The influence of hydroxyl orientation, stacking, and ionic substitutions on the interlayer bonding of micas. *Clays and Clay Minerals*, 25, 102–104.
- (1978) The electrostatic interlayer forces of layer structure minerals. *Clays and Clay Minerals*, 26, 51–57.
- González-Elipe, A.R., Espinós, J.P., Munuera, G., Sanz, J., and Serratos, J.M. (1988) Bonding-state characterization of constituent elements in phyllosilicate minerals by XPS and NMR. *Journal of Physics and Chemistry*, 92, 3471–3476.
- Griffith, A.A. (1921) The phenomena of rupture and flow in solids. *Philosophical Transactions of the Royal Society of London, Series A*, 221, 163–198.
- Guggenheim, S., Chang, Y.-H., and Koster van Groos, A.F. (1987) Muscovite dehydroxylation: High-temperature studies. *American Mineralogist*, 72, 537–550.
- Guidotti, C.V., Sassi, F.P., Comodi, P., Zanazzi, P.F., and Blencoe, J.G. (2005) Slaty cleavage: does the crystal chemistry of layer silicates play a role in its development? *Canadian Mineralogist*, 43, 311–325.
- Gutshall, P.L., Bryant, P.J., and Cole, G.M. (1970) Cleavage surface energy of phlogopite mica. *American Mineralogist*, 55, 1432–1434.
- Guven, N. (1971) The crystal structures of 2M₁ phengite and 2M₁ muscovite. *Zeitschrift für Kristallographie*, 134, 196–212.
- Hazen, R.M., and Burnham, C.W. (1973) The crystal structures of one-layer phlogopite and annite. *American Mineralogist*, 58, 889–900.
- Hazen, R.M., Finger, L.W., and Velde, D. (1981) Crystal structure of a silica- and alkali-rich trioctahedral mica. *American Mineralogist*, 66, 586–591.
- Heinz, H. (2006) Interaction energy and surface reconstruction between sheets of layered silicates. *The Journal of Chemical Physics*, 124, 224713.
- Heinz, H., Koerner, H., Anderson, K.L., Vaia, R.A., and Farmer, B.L. (2005) Force field for mica-type silicates and dynamics of octadecylammonium chains grafted to montmorillonite. *Chemistry of Materials*, 17, 5658–5669.
- Heinz, H., Lin, T.J., Mishra, R.K., and Emami, F.S. (2013) Thermodynamically consistent force fields for the assembly of inorganic, organic, and biological nanostructures: the interface force field. *Langmuir*, 29, 1754–1765.
- Hochella, M.F. Jr. (1990) Atomic structure, microtopography, composition, and reactivity of mineral surfaces. In M.F. Hochella and A.F. White, Eds., *Mineral-Water Interface Geochemistry*, 27, p. 87–132. Reviews in Mineralogy, Mineralogical Society of America, Chantilly, Virginia.
- (1995) Mineral surfaces: their characterization and their chemical, physical and reactive nature. In D.J. Vaughan and R.A.D. Patnick, Eds., *Mineral Surfaces*, 5, 17–60. The Mineralogical Society Series.
- Kogel, J.E., Krukowsk, S.T., Trivedi, N.C., and Barker, J.M. (2006) Industrial Minerals and Rocks: Commodities, Markets, and Uses, 1548 pp. Society for Mining Metallurgy and Exploration, Littleton, Colorado.
- Kogure, T. (1997) On the structure of cleaved surface in biotite mica. *Mineralogical Journal*, 19, 155–164.
- Kuwahara, Y. (2001) Comparison of the surface structure of the tetrahedral sheets of phlogopite and muscovite by AFM. *Physics and Chemistry of Minerals*, 28, 1–8.
- Irwin, G. (1957) Analysis of stresses and strains near the end of a crack traversing a plate. *Journal of Applied Mechanics*, 24, 361–364.
- Laurora, A., Brigatti, M.F., Mottana, A., Malferrari, D., and Caprilli, E. (2007) Crystal chemistry of trioctahedral micas in alkaline and subalkaline volcanic rocks: A case study from Mt. Sassetto (Tolfa district, Latium, central Italy). *American Mineralogist*, 92, 468–480.
- Laurora, A., Malferrari, D., Brigatti, M.F., Mottana, A., Caprilli, E., Giordano, G., and Funicello, R. (2009) Crystal chemistry of trioctahedral micas in the top sequences of the Colli Albani volcano, Roman Region, central Italy. *Lithos*, 113, 507–520.
- Lazar, P., and Podloucky, R. (2008) Cleavage fracture of a crystal: Density functional theory calculations based on a model which includes structural relaxations. *Physical Review B: Condensed Matter and Materials Physics*, 78, 104114.
- Lazar, P., Podloucky, R., and Wolf, W. (2005) Correlating elasticity and cleavage. *Applied Physics Letters*, 87, 261910.
- Lin, C.-Y., and Bailey, S.W. (1984) The crystal structure of paragonite-2M₁. *American Mineralogist*, 69, 122–127.
- Matarrese, S., Schingaro, E., Scordari, F., Stoppa, F., Rosatelli, G., Pedrazzi, G., and Ottolini, L. (2008) Crystal chemistry of phlogopite from Vulture-S. Michele Subsynthetite volcanic rocks (Mt. Vulture, Italy) and volcanological implications. *American Mineralogist*, 93, 426–437.
- Maurice, P.A. (2009) Environmental Surfaces and Interfaces from the Nanoscale to the Global Scale, 441 pp. Wiley.
- McCaughey, J.W., Newnham, R.E., and Gibbs, G.V. (1973) Crystal structure analysis of synthetic fluorophlogopite. *American Mineralogist*, 58, 249–254.
- Ohta, T., Takeda, H., and Takéuchi, Y. (1982) Mica polytypism: similarities in the crystal structures of coexisting 1M and 2M₁ oxybiotite. *American Mineralogist*, 67, 298–310.
- Parks, G.A. (1984) Surface and interfacial free energies of quartz. *Journal of Geophysical Research: Solid Earth*, 89, 3997–4008.
- Poppa, K., and Elliot, G. (1971) The surface composition of mica substrates. *Surface Science*, 24, 149–163.
- Pugno, N.M., and Ruoff, R.S. (2004) Quantized fracture mechanics. *Philosophical Magazine*, 84, 2829–2845.
- Redhammer, G.J., and Roth, G. (2002) Single-crystal structure refinements and crystal chemistry of synthetic trioctahedral micas KM₃(Al³⁺, Si⁴⁺)₃O₁₀(OH)₂, where M = Ni²⁺, Mg²⁺, Co²⁺, Fe²⁺, or Al³⁺. *American Mineralogist*, 87, 1464–1476.
- Russell, R.L., and Guggenheim, S. (1999) Crystal structures of hydroxyphlogopite at high temperatures and heat-treated biotites: The influence of the O, OH, F site. *Canadian Mineralogist*, 37, 711–720.
- Schingaro, E., Mesto, E., Scordari, F., Brigatti, M.F., and Pedrazzi, G. (2005) Cation site partitioning in Ti-rich micas from Black Hill (Australia): a multi-technical approach. *Clays and Clay Minerals*, 53, 179–189.
- Scordari, F., Ventruti, G., Sabato, A., Bellatreccia, F., Della Ventura, G., and Pedrazzi, G. (2006) Ti-rich phlogopite from Monte Vulture (Potenza, Italy) investigated by a multi-analytical approach: substitutional mechanisms and orientation of the OH dipoles. *European Journal of Mineralogy*, 18, 379–391.
- Scordari, F., Schingaro, E., Ventruti, G., Lacalmita, M., and Ottolini, L. (2008) Red micas from basal ignimbrites of Mt. Vulture (Italy): interlayer content appraisal by a multi-methodic approach. *Physics and Chemistry of Minerals*, 35, 163–174.
- Zhang, S., Zhu, T., and Belytschko, T. (2007) Atomistic and multiscale analyses of brittle fracture in crystal lattices. *Physical Review B: Condensed Matter and Materials Physics*, 76, 094114.